EDGE ARTICLE

Check for updates

Bispidine as a β-strand nucleator: from a β-arch to self-assembled cages and vesicles†

Hanuman Singh, [a] Akshay Chenna, [b] Upanshu Gangwar, [a] Julie Borah, [b] Gaurav Goel *[b] and V. Haridas *[a]

The development of synthetic scaffolds that nucleate well-folded secondary structures is highly challenging. Herein, we designed and synthesized a series of core-modified peptides (**F1**, **F2**, **F3**, and **F4**) that fold into β-strand structures. These bispidine-scaffolded peptides were studied by CD, IR, NMR, single crystal XRD, and Molecular Dynamics (MD) simulations to investigate their conformational preferences. Solid-state and solution studies revealed that bispidine is a versatile scaffold that could be placed either at the terminal or at the middle of the peptide strand for nucleating the β-strand structure. Scaffolds that nucleate an isolated β-strand conformation are rare. Bispidine placed at the C-terminus of the peptide chain could nucleate a β-strand conformation, while bispidine placed at the middle resulted in a β-arch conformation. This nucleation activity stems from the ability to restrict the psi torsion angle (ψ) through intramolecular C5 hydrogen bonding between the equatorial hydrogen(s) of bispidine and the carbonyl oxygen(s) of the amino acid close to the scaffold. Furthermore, the bispidine peptidomimetic with a super secondary structure, namely β-arch, assembled into single-hole submicron cages and spherical vesicles as evident from microscopic studies. The design logic defined here will be a significant strategy for the development of β-strand mimetics and super secondary structures.

Introduction

Proteins have uniquely folded secondary structures (α-helix and β-strand) that undergo well-controlled self-assembly to form hierarchically ordered assemblies. This supramolecular assembly called a quaternary structure ranges from nanometers to micrometers and beyond.[1] The functional aspect of proteins is intimately linked to their secondary and quaternary structures. However, the evolution of the quaternary structure from the secondary structure is not well understood.[2] In addition, the development of biomimetic systems with the ability to form a sophisticated assembly will have far-reaching applications in areas like therapeutics, and in the development of artificial enzymes.[3,4] In this perspective, the *de novo* design of secondary structure mimetics with the ability to self-assemble has multiple applications. The secondary structure mimetics can act as an effective agent to perturb protein–protein interactions (PPIs)[5] and are expected to be useful in studying bioactive conformations. Many studies have already explored α-helix mimics while β-sheet mimics are less studied because of the

lack of good chemical models.[6–9] Similarly, helical PPIs have been extensively targeted, while the inhibition of the β-sheet interface is very limited.[10] Peptidomimetic foldamers that can mimic β-sheet interfaces and form soluble β-sheet aggregates can be excellent candidates for therapeutic intervention against protein aggregation.[11] However, in general, short peptides do not have a single dominant solution conformation. The insertion of an unnatural backbone in the peptide sequence is a better strategy to overcome these issues. The groups of Kelly,[12] Nowick,[13] Hamilton,[14] and Gellman[15] have designed various β-sheet peptidomimetics.

Scaffolds that could enforce peptide conformation to specific secondary structures such as an α-helix or β-sheet are scarce. The nucleation of secondary structures is achieved by the introduction of a rigid unit that favors the initial hydrogen-bonding pattern of the α-helix or β-strand as per the nucleating preference of the scaffold.[6–9,16–18] However, there are limited examples of isolated β-strands. Most of the designed scaffolds act by facilitating initial hydrogen bonding to form a sheet that further propagates the β-sheet structure. Furthermore, turns are proposed to be the nucleators of secondary structures without loss in chain entropy.[19] Bispidine serves as a versatile scaffold for nucleating secondary structures such as reverse turns, helices, and sheets in peptides.[20,21] The nature of the linkage between the peptide fragments and the bispidine scaffold is crucial for nucleating specific secondary structures. Here we show that bispidine could nucleate isolated β-strand and β-arch

a Department of Chemistry, Indian Institute of Technology Delhi, Hauz Khas, New Delhi-110016, India. E-mail: haridasv@chemistry.iitd.ac.in

b Department of Chemical Engineering, Indian Institute of Technology Delhi, Hauz Khas, New Delhi-110016, India. E-mail: goelg@chemical.iitd.ac.in

super secondary structure along with their intrinsic ability to self-assemble. The unique geometry of the bispidine scaffold facilitates intramolecular C5-hydrogen bonding, thereby nucleating the β-strand structure on the attached peptides. Bispidine could be placed either at the C-terminus of the peptide or in the middle of the peptide strand for nucleating the β-strand.

Results and discussion

We show that the introduction of an artificial rigid structure that enables chain reversal could lead to the nucleation of secondary structures. In this report, we incorporate a rigid bicyclic entity reminiscent of an artificial turn in a peptide. The bispidine unit could be considered as a folded diaminopropane due to its bicyclic architecture (Fig. 1). This bicyclic unit could be considered as a turn since it provides a kink to the peptide backbone. Bispidine could be attached to the peptide portion through amide bonds between the amino units of bispidine and the C-terminal of peptide fragments. The bispidine scaffold can be synthesized easily and allows easy incorporation of peptide units.

Herein, we incorporated bispidine as a non-peptidic molecular scaffold that can act as a promising template for the nucleation of β-strand secondary structures and further assemble into a vesicular quaternary structure. Bispidine was synthesized from Boc protected piperidone, benzylamine, and formaldehyde through a double Mannich reaction, followed by Wolff–Kishner reduction. The bispidine peptide conjugate adopts a conformation based on the nature of the linkage between the peptide and scaffold.[20,21] Bispidine was incorporated into the peptide by a typical peptide coupling procedure (Scheme S1†). A series of bispidine–peptide conjugates with an increasing number of amino acids were designed and synthesized (Fig. 2). A dipeptide **F1**, tetrapeptide **F2**, hexapeptide **F3**, and deprotected water-soluble hexapeptide **F4** were chosen for conformational studies. The conformations of bispidine
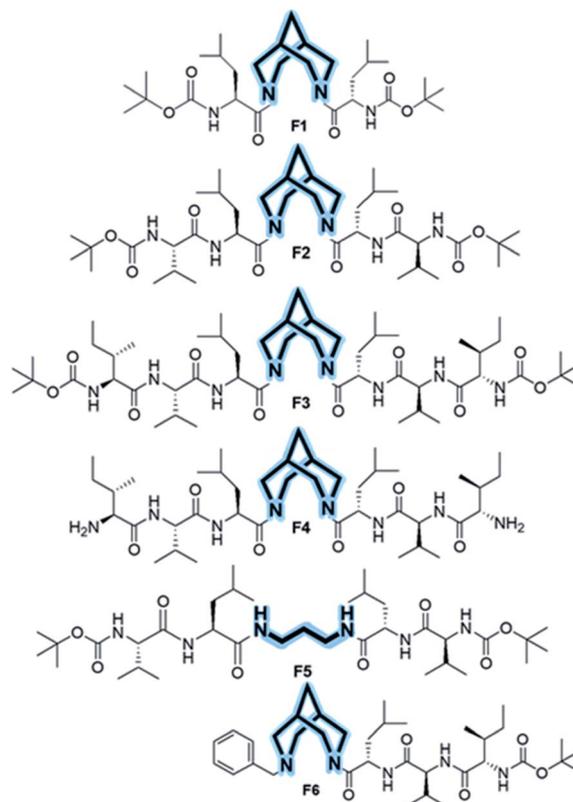

Fig. 2 Chemical structures of foldamers (**F1–F4**) in which the bispidine scaffold is at the middle. Control compound **F5** with a 1,3 diaminopropane spacer instead of bispidine and **F6** with bispidine placed at the terminal.

peptide conjugates **F2–F4** were studied by CD, 1D, and 2D NMR, variable temperature NMR (VT-NMR), FT-IR, and all-atom MD simulations. The crystallographic coordinates of **F1** were used to create an initial structure for MD simulations of bispidine anchored peptides (simulation details in Section S 2.1†). For each system, we generated a 200 ns trajectory and calculated averages from the last 50 ns portion. All structural properties, such as the distribution of (φ, ψ) dihedrals, converged on the simulation time scale (Fig. S11†).

The ^{1}H NMR spectra of **F2** and **F3** showed two interconverting conformers, *syn* and *anti*. The J1,3-coupling values of amide NHs of both *syn* and *anti*-forms are in the range 8–9 Hz (Tables S1 and S7†), suggesting an extended β-strand conformation in both *syn* and *anti*-forms as observed from ^{1}H NMR and MD simulations.[22,23] The chemical shifts of the α-protons for all amino acid residues of bispidine-linked compounds are downfield shifted with respect to the random coil structure indicating β-strand structures (Table S2†).[15] The bispidine scaffold adopts a double chair conformation, with the distance between the nitrogen atoms at around 2.9 Å. The rotation of the carbonyl units can result in four conformers, two *anti* (a1 and a2′) and two *syn* (s1 and s2′) (Fig. S1†). The *syn* and *anti*-forms are readily observable in the ^{1}H NMR spectra of bispidine conjugates.[20] In CDCl$_3$, the ratio of *anti* to *syn* was 3 : 1, while DMSO favored the structure with a high dipole moment, the *syn*
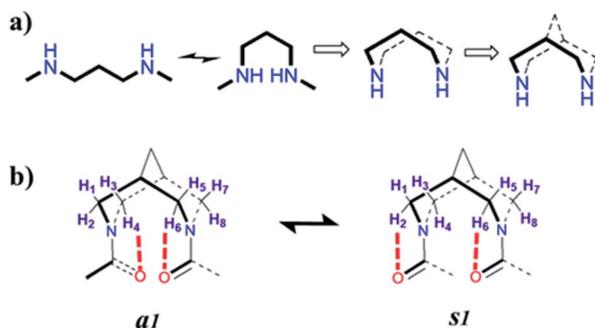

Fig. 1 Evolution of the bispidine scaffold. (a) The most preferred conformer of the 1,3-diaminopropane linker along with the folded conformer. Cyclization of this folded conformer results in conformational restriction. This cyclic structure is further interlocked by a methylene bridge resulting in a bicyclic architecture. (b) The conformations of bispidine diamides, showing the equatorial hydrogen atoms that are proximal to the carbonyl oxygen atoms. The *anti* (a1) and *syn* (s1) forms are shown.

conformer.[24,25] The ROESY spectrum confirmed the presence of *syn* and *anti*-conformers in **F3** (Fig. 3a and b).

The exchange rate is obtained by performing selective and non-selective inversion recovery experiments[26] under varying temperature ranges to get the thermodynamic parameters. The calculated rate constants were fitted using the Arrhenius and the Eyring equations resulting in an activation energy barrier ($\Delta E^{\ddagger}$) and a standard enthalpy of activation ($\Delta H^{\ddagger}$) between *syn* and *anti*-conformers equal to 110.08 kJ mol^{-1} and 107.67 kJ mol^{-1}, respectively (Fig. S2a–c, Tables S4 and S5†). This molecular switching behavior of bispidine diamides is analogous to the peptide bond isomerization of proline-containing peptides. Prolyl isomerization plays a key role in protein folding and in the cell signaling process.[27,28] The $\Delta E^{\ddagger}$ and $\Delta H^{\ddagger}$ values of bispidine compounds are comparable to the *cis–trans* isomerization of proline peptides, and hence bispidine could serve as a scaffold in the design of artificial functional switching peptide systems.

^{1}H NMR studies revealed that all amide NHs appeared at <7.0 ppm in **F2** and **F3** indicating that they are non-hydrogen bonded, since the hydrogen-bonded amide NH usually appears around 8.0 ppm in CDCl$_3$ solution.[29,30] The VT-NMR studies on compound **F3** in CDCl$_3$ revealed $\Delta\delta/\Delta t$ in the range −0.004 to −0.006 ppm per K (Fig. S3†) for the amide NH, indicating the absence of intramolecular hydrogen bonding.[31,32] Furthermore, the FT-IR spectrum of **F2** and **F3** in chloroform solution showed a band at 3438 and 3435 cm^{-1} respectively (Fig. S6c and d†), again indicating that the predominant form in solution is non-bonded NHs. The addition of a hydrogen bond accepting solvent like DMSO-d_6 to CDCl$_3$ solutions of peptides **F2** and **F3** resulted in significant chemical shift changes of amide NHs (Fig. S4†). All amide NHs in **F2** and **F3** are solvent-exposed as evident from the relatively high chemical shift values of NHs upon addition of DMSO-d_6. These orthogonal measurements confirm the absence of intramolecular hydrogen bonds, as also corroborated by the MD simulation of **F3** in CHCl$_3$ wherein we obtained only 0.28 intramolecular H bonds (involving NHs) per molecule (Table S11†).[33]

The ROESY spectra of compounds **F2** and **F3** showed strong ROE between C$_\alpha$Hs of Leu and equatorial hydrogens of bispidine (Fig. 3a, b, and S5a–g†), a significant observation that is discussed later. Furthermore, all NHs showed strong ROE with neighboring C$_\alpha$Hs, supporting a β-strand structure. Additionally, the amide I stretching of **F2** and **F3** showed a band at 1637 and 1633 cm^{-1} respectively, indicating that it is predominantly in the β-strand conformation (Fig. S6a and b†).[35,36] This is also evident from MD simulations as the inter-proton distances between neighboring amide hydrogens are under 3 Å indicative of a β-strand (Fig. S13†).[37] Our simulations reveal that the stable solution structure of **F3** in all three solvents used here, *viz.*, chloroform, methanol, and water, has an extended conformation (Fig. 4a and Table S7†) with all backbone torsional angles having a high population in the β-sheet region (Fig. 4b and Table S8†).

The CD spectrum of compounds **F1**, **F2**, and **F3** in methanol showed a positive maximum at ∼197 nm and a negative band around 226 nm (Fig. 3c), indicating the presence of a β-strand conformation in all three compounds. The shift from the typical
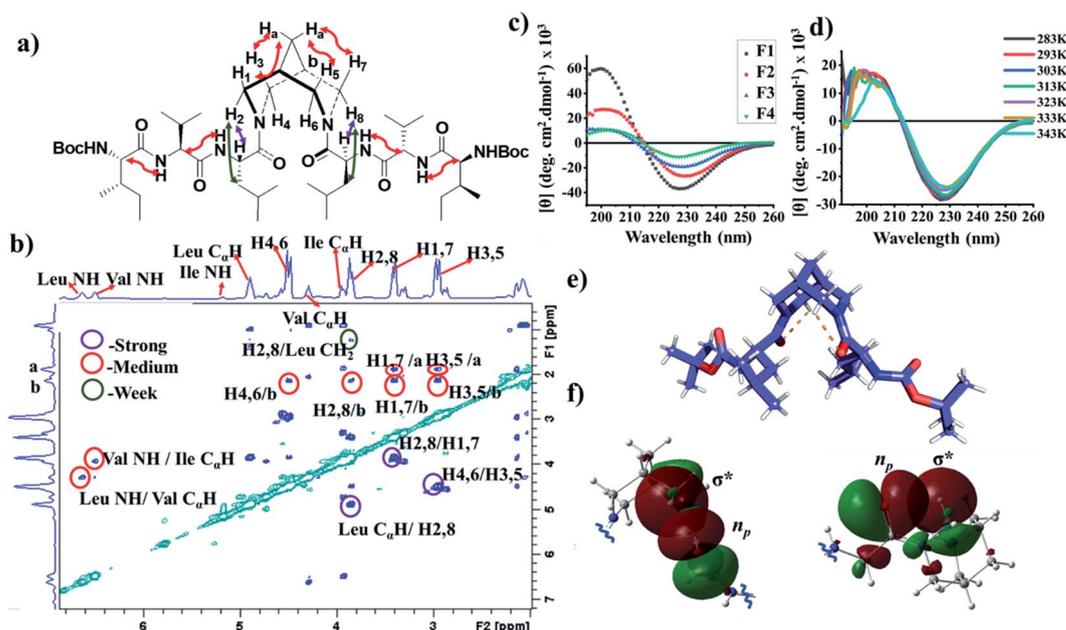
Fig. 3 (a) The ROE observation in molecule **F3**. (b) A cross section of the ROESY spectrum of **F3** in chloroform showing the correlation between the peptide chain and the bispidine linker. (c) Circular dichroism (CD) spectrum of compounds **F1**, **F2**, and **F3** in methanol, and **F4** in water. (d) Temperature-dependent CD of compound **F3**. (e) X-ray crystal structure of compound **F1** showing intramolecular H-bonding between Leu carbonyl and bispidine equatorial hydrogen (C−H⋯O). (f) The orbital view of C5−hydrogen bonding in the crystal structure of **F1**. The lone pair containing p-type orbital of carbonyl oxygen interacts with the C−H σ* orbital. The two colors (red and green) show the two phases (positive and negative) of molecular orbitals, respectively.

β-sheet CD is not uncommon in synthetic peptides.[38–40] A water-soluble version of the bispidine–peptide conjugate was also synthesized by deprotecting the terminal Boc groups. The water-soluble amine derivate **F4** showed a similar CD spectrum as that of **F2** and **F3** (Fig. 3c and Table S8†). The temperature-dependent CD of **F3** from 0 °C to 70 °C showed no significant changes (Fig. 3d and S7a†), indicating a highly robust secondary structure of these peptides.[41] The β-strand conformation is devoid of extensive hydrogen bonds, and therefore, shows a weak temperature dependence. The representative conformation of **F1**, **F2**, **F3**, and **F4** is a β-arch type structure.[42] In this case, the two β-stands are isolated with bispidine at the middle, which acts as a turn. The angle between the two β-strands is 150°. The bispidine linker that connects two parallel β-strands could adopt a *syn*- or *anti*-form. The *syn* form keeps the parallel β-strands with their faces on the same side, while the anti-form keeps the faces of β-strands in opposite directions. A 2D potential energy scan on torsional angles O30–C2–N31–C19 and O29–C3–N23–C1 in the gas phase, obtained using quantum mechanical calculations with B3LYP/6-31G*, revealed the *anti*- and the *syn*-forms as the lowest energy states (*anti* more stable than *syn*) (Fig. S15†). The topological placement of β-strands is important, since one face or both faces of the β-strand could be involved in interaction with the target protein.[43] The bispidine scaffold providing various topological arrangements of β-strands (Fig. S14†) is an added advantage. The β-arch motif is found in the amyloid-forming fibrillar assemblies and also in β-solenoid proteins.[44]

To evaluate the nucleating effect when bispidine is placed at the terminus, compound **F6** was synthesized (Scheme S3†). The CD spectrum of **F6** revealed the presence of a β-strand conformation (Fig. S7b†). MD simulations also show that the solution structure of **F6** is essentially the same as that of **F3**: a β-strand conformation with main chain (φ and ψ) angles predominantly in the β region (Table S8†) and $^3J_{HNH\alpha}$ values (>8 Hz) also equivalent to those in **F3** (Table S7†). To understand the reason behind the nucleation of the β-strand by bispidine, a control compound **F5** (tetrapeptide with 1,3-diaminopropane as the spacer) was synthesized (Scheme S2†), while a similar control compound **F7** (hexapeptide with 1,3-diaminopropane as the spacer) was used for MD simulations. The unique role of bispidine as a β-strand inducer is evident from the following observations: the CD spectrum of **F5** showed no characteristic secondary structure (Fig. S7c†), the chemical shift value of $C_\alpha H$ in **F5** is comparable to the random coil structure[15] unlike bispidine-linked compounds (Table S3†), and the population of the main chain (φ and ψ) angles of Leu, Val, and Ile in the β-strand region was 98%, 30%, and 60% for **F3**, while it was only 14%, 8%, and 6% for **F7**, respectively (Fig. 4b and Table S8†).

The X-ray crystal structure of **F1** gave an insight into the unique role of bispidine as a β-strand nucleator. The distance between Leu carbonyl and bispidine equatorial hydrogens (H4,6 in the *anti*-form, Fig. S5e;† H2,6 in the *syn* form, Fig. S5f†) was 2.4 Å with a donor and acceptor angle $\langle$CHO $\rangle$ 90° (Table S10†), thus satisfying the C–H···O hydrogen bond criterion (d_{H-O} < 2.7 Å and $\langle$CHO$\rangle$ 90°).[45] This implies that bispidine could restrict
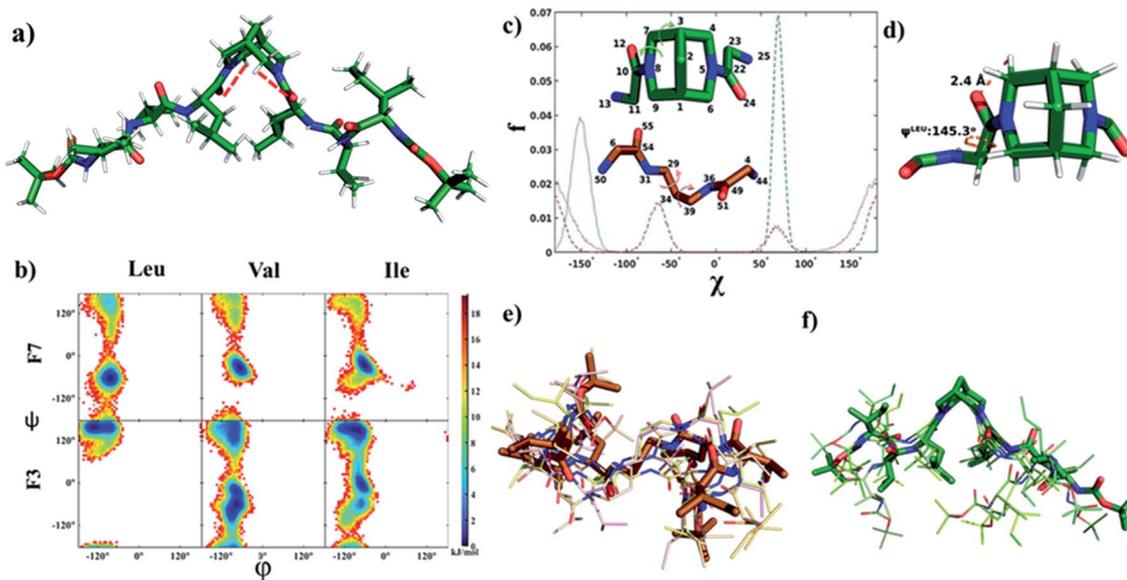

Fig. 4 (a) Solution structure of **F3** in chloroform obtained from MD simulation (intramolecular C–H···O bond between Leu carbonyl and bispidine equatorial hydrogen is shown by a dashed red line. (b) Density plot of the population (fraction *f* reported in the units of free energy $-RT \ln f$) of main-chain torsion angles (φ and ψ) obtained from the MD simulation of a single molecule of **F3** (consisting of a bispidine linker) or **F7** (consisting of a 1,3 diaminopropane linker) in chloroform. A significant shift to the characteristic β-strand region ($\varphi \sim -140°$ and $\psi \sim 130°$) is seen for all residues of **F3**. (c) Comparison of the distribution of the two torsion angles (shown in the inset) capturing the linker conformational space: C22–N5–C6–C1 (solid green) and N5–C6–C1–C9 (dashed green) in **F3**, C54–N31–C29–C34 (solid brown) and N31–C29–C34–C39 (dashed brown) in **F6**. (d) A representative snapshot showing the main chain ψ dihedral of leucine, and the C–H···O bond between bispidine equatorial hydrogen (atom 77) and leucine carbonyl oxygen (atom 24) in **F3**. (e and f) Overlay of the central structures of the five most populated clusters of **F7** and **F3**, respectively (cluster population in Table S9†), obtained from the equilibrium portion of MD trajectory using the Gromos algorithm[34] with a backbone root mean squared deviation (RMSD) cut-off of 0.1 nm.

the ψ angle of the connected residue (Leu) by C5-hydrogen bonding (Fig. 3e and Table S6†). These structural features were also present in the solution state structure of **F3** (bispidine hexapeptide) and **F6** (terminal bispidine tripeptide), as determined from MD simulations. The average distance between the carbonyl oxygen of Leu and equatorial hydrogens of bispidine was found to be ~2.5 Å (Fig. 4d and Table S10†), and the average number of C–H⋯O bonds per tripeptide arm was found to be 0.77 in **F3** and 0.71 in **F6**, while it was only 0.27 in **F7** (Table S11 and Fig. S12†). **F3** and **F6** also show significantly higher preference than **F7** for a β-strand geometry, consistent with the role of C5 hydrogen bonding in stabilizing the protein β-strand secondary structure.[46]

The orbital analysis of the X-ray structure of **F1** was performed by using the Gaussian package,[47,48] which showed the overlap of the p-type orbital of carbonyl oxygen with the C–H σ* orbital (Fig. 3f). We also analyzed X-ray crystal structures of several bispidine diamides that further supported similar orbital interactions (Fig. 3f). Computational analysis of the rotation of diamides such as simple diacetyl derivatives revealed *syn*- and *anti*-forms that are stabilized by intramolecular C–H⋯O hydrogen bonding (Table S12†). We envisioned that the C–H⋯O interaction could preorganize the first residue, thereby reducing the number of conformations that the polypeptide can adopt; hence decreasing the entropy cost of folding. Unlike the bispidine scaffold, the diaminopropane spacer itself has considerably higher conformational flexibility: Schlitter's entropy, calculated from the covariance matrix of position fluctuations for N–C–C–C–N atoms in the MD trajectory, was 0.24 J (mol K)$^{-1}$ for **F3** and 1.16 J (mol K)$^{-1}$ for **F7**. This higher flexibility of **F7** compared with **F3** is evident from the sampling of multiple conformational substates of the linker (Fig. 4c) as well as a wider sampling of the whole molecule (Fig. 4e and f), which can be attributed to the lack of a well-defined secondary structure in **F7**. The initial preorganization provided by the scaffold through two C–H⋯O interactions could lead to cooperativity in folding. The four conformational states in bispidine diamides are stabilized by non-canonical intramolecular C–H⋯O hydrogen bonding, hence making many of the possible orientations of carbonyls unfavorable. A pair of non-canonical interactions between the scaffold and amino acid carbonyl preorganize the peptide strand.

The energy diagram of the rotation of amide carbonyls clearly shows the minima at *syn*- and *anti*-states (Fig. S15†). The two peptide strands separated by bispidine adopt an independent albeit identical conformation, and the different rotamer forms of bispidine (two *anti* and two *syn*) do not appear to affect the strand conformation. We obtained an equal number of C–H⋯O hydrogen bonds (2), a similar value for the Leu-ψ angle (153°–162°), and the same secondary structure assignment (β) for all four metastable conformations of **F1** determined from quantum chemical calculations (Table S12†). Also, a backbone RMSD of 0.8 ± 0.2 Å was obtained between the peptide strands in the *syn*- and the *anti*-states of **F3** in chloroform. The C5 hydrogen bonding was present in both *syn*- and *anti*-forms (Fig. S12a and b†), which in-turn could constrain the conformation of bispidine anchored peptides. Therefore, even though

these rotamers are observed as a result of slow rotation on the NMR time scale, both conformers are identically locked by intramolecular H-bonding. The non-canonical tethering by the bispidine scaffold could control the ψ dihedral angle of the residue adjacent to it and this conformational preference is propagated to the remaining residues (Table S8†). Therefore, the lack of C5 hydrogen bonding in diaminopropane spacer-linked compounds could be directly linked to the absence of β-strand geometry in them.

The link between secondary and quaternary structures is the holy grail of biomolecular interactions. The coiled-coil structure of keratin and the assembly of poly-proline helices in collagen highlight how the secondary structure leads to a functional assembly.[49,50] The engineering of the secondary structure itself is a surmountable challenge, while the assembly from an engineered secondary structure into a defined quaternary structure is a formidable task.

In order to investigate the self-assembly of the β-arch mimetic, detailed ultramicroscopic imaging such as scanning electron microscopy (SEM), transmission electron microscopy (TEM), and atomic force microscopy (AFM) is performed. At 0.25 mg ml^{-1} concentration of **F2**, single orifice cages are observed (Fig. 5a) with the size of hollow cages ranging from 150 to 400 nm (Fig. S9a†). This is similar to single-hole nanocages reported in mesoporous silver and polymeric materials.[51] Molecular containers such as cucurbiturils[52] and cyclodextrins[53] were extensively used for the encapsulation of a variety of molecules and served as chemical models for studying enzyme mechanisms. In these molecular containers, two sides are open, while our self-assembled systems provide more possibilities for various topologies and dimensions.

Self-assembled systems offer advantages in terms of controlling the size by engineering building blocks. In addition to that, the confined space could be used for performing chemical reactions. Self-assembled peptide nanotubes and peptide-based vesicles have several applications.[54–56] For example, protein nanocages are versatile platforms for nanotechnology applications.[57] Here, we found that increasing **F2** concentration to 0.5 mg ml^{-1} resulted in the formation of vesicles with sizes ranging from 400 nm to 1200 nm (Fig. 5b and S9b†). The fine-tuning of self-assembled structures like single-hole cages and vesicles by changing the concentration will be useful in controlled encapsulation and delivery. The results obtained from SEM analysis are consistent with other measurements. For example, TEM of **F2** also revealed single-hole submicron cages at a concentration of 0.25 mg ml^{-1} (Fig. 5c).

Increasing the concentration to 0.5 mg ml^{-1} resulted in complete vesicle formation (Fig. 5d). AFM imaging of **F2** also showed single-hole submicron cages at a concentration of 0.25 mg ml^{-1} (Fig. 5e) and vesicles at 0.5 mg ml^{-1} (Fig. 5e, f, S8c and d†). Size distribution analysis using dynamic light scattering (DLS) based studies also reveals that the average size of single-hole cages lies in the range 200 to 600 nm at 0.25 mg ml^{-1} and the average size of vesicles lies in the range 400 to 900 nm in solution (Fig. S10a and b†). Similarly, **F3** showed vesicular assembly in methanol at 0.5 mg ml^{-1} with sizes ranging from 200 nm to 800 nm (Fig. S8b and S9c†). The self-assembly of **F5** was also investigated by SEM and it showed no vesicular
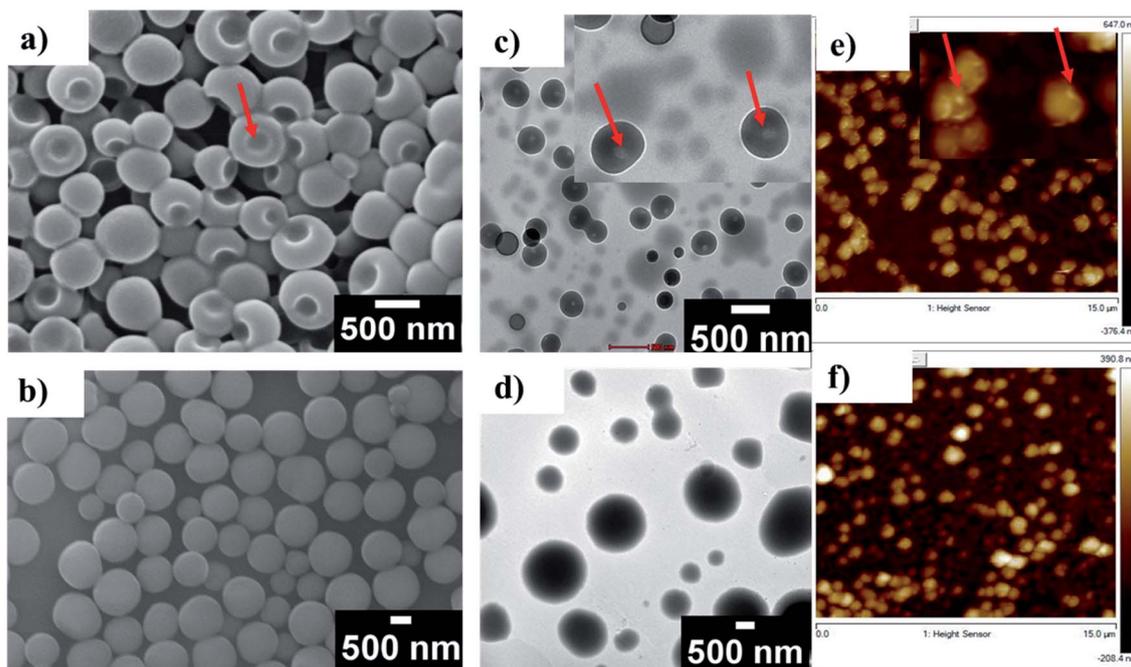
Fig. 5 (a) SEM of **F2** at 0.25 mg ml^{-1}. (b) SEM of **F2** at 0.5 mg ml^{-1}. (c) TEM of **F2** at 0.25 mg ml^{-1} (red arrows indicate the hole). (d) TEM of **F2** at 0.5 mg ml^{-1}. (e) AFM of **F2** at 0.25 mg ml^{-1} (red arrows indicate the hole). (f) AFM of **F2** at 0.5 mg ml^{-1}.

assembly (Fig. S8a†), which confirms that bispidine has a significant role in the formation of vesicles *via* the self-assembly of β-strands.

Conclusions

By using integrative experimental structure determination techniques combined with MD simulations, we showed that using the scaffolding approach, short peptides could be folded into a well-defined and stable β-strand conformation. This forced folding of peptides using a bicyclic scaffold, bispidine, is a versatile approach. In this approach, the C5 hydrogen bonding between the scaffold and the first residue resulted in the restriction of the ψ angle that further propagated and controlled the conformation of the peptide. Our strategy, wherein, one could induce a β-strand in a peptide, will be a powerful strategy in protein engineering. The self-assembly of the beta strand-turn-beta strand secondary structure into higher-ordered structures such as single-hole submicron cages and vesicles is an additional aspect that is expected to find applications in drug delivery.

Data availability

All synthetic procedures, MD simulations, and NMR data supporting this article are in the ESI.†

Author contributions

This manuscript was written through the contributions of all authors. HS designed, synthesized, characterized, and studied the conformation and self-assembly of all the compounds under the supervision of VH. AC and JB performed the simulations under the supervision of GG. Dynamic NMR studies were performed by UG.

Conflicts of interest

There are no conflicts to declare.

Acknowledgements

Notes and references

1 M. H. Barbee, Z. M. Wright, B. P. Allen, H. F. Taylor, E. F. Patteson and A. S. Knight, *Macromolecules*, 2021, **54**, 3585–3612.

2 W. S. Horne and T. N. Grossmann, *Nat. Chem.*, 2020, **12**, 331–337.

3 T. A. Martinek, A. Hetényi, L. Fülöp, I. M. Mándity, G. K. Tóth, I. Dékány and F. Fülöp, *Angew. Chem., Int. Ed.*, 2006, **45**, 2396–2400.

4 J. Eom, J. Gong, S. Kwon, A. Jeon, R. Jeong, R. W. Driver and H. Lee, *Angew. Chem., Int. Ed.*, 2015, **54**, 13204–13207.

5 L.-G. Milroy, T. N. Grossmann, S. Hennig, L. Brunsveld and C. Ottmann, *Chem. Rev.*, 2014, **114**, 4695–4748.

6 J. M. Davis, L. K. Tsou and A. D. Hamilton, *Chem. Soc. Rev.*, 2007, **36**, 326–334.

7 V. Haridas, *Eur. J. Org. Chem.*, 2009, **2009**, 5112–5128.

8 L. Cussol, L. Mauran-Ambrosino, J. Buratto, A. Y. Belorusova, M. Neuville, J. Osz, S. Fribourg, J. Fremaux, C. Dolain, S. R. Goudreau, N. Rochel and G. Guichard, *Angew. Chem., Int. Ed.*, 2021, **60**, 2296–2303.

9 H. N. Hoang, C. Wu, T. A. Hill, A. Dantas de Araujo, P. V. Bernhardt, L. Liu and D. P. Fairlie, *Angew. Chem., Int. Ed.*, 2019, **58**, 18873–18877.

10 V. Azzarito, K. Long, N. S. Murphy and A. J. Wilson, *Nat. Chem.*, 2013, **5**, 161–173.

11 A. M. Watkins and P. S. Arora, *ACS Chem. Biol.*, 2014, **9**, 1747–1754.

12 R. Kaul, A. R. Angeles, M. Jäger, E. T. Powers and J. W. Kelly, *J. Am. Chem. Soc.*, 2001, **123**, 5206–5212.

13 A. G. Kreutzer, S. Yoo, R. K. Spencer and J. S. Nowick, *J. Am. Chem. Soc.*, 2017, **139**, 966–975.

14 H. Lingard, J. T. Han, A. L. Thompson, I. K. H. Leung, R. T. W. Scott, S. Thompson and A. D. Hamilton, *Angew. Chem., Int. Ed.*, 2014, **53**, 3650–3653.

15 F. Freire and S. H. Gellman, *J. Am. Chem. Soc.*, 2009, **131**, 7970–7972.

16 S. T. Phillips, M. Rezac, U. Abel, M. Kossenjans and P. A. Bartlett, *J. Am. Chem. Soc.*, 2002, **124**, 58–66.

17 P. N. Wyrembak and A. D. Hamilton, *J. Am. Chem. Soc.*, 2009, **131**, 4566–4567.

18 A. B. Smith, T. P. Keenan, R. C. Holcomb, P. A. Sprengeler, M. C. Guzman, J. L. Wood, P. J. Carroll and R. Hirschmann, *J. Am. Chem. Soc.*, 1992, **114**, 10672–10674.

19 A. M. C. Marcelino and L. M. Gierasch, *Biopolymers*, 2008, **89**, 380–391.

20 V. Haridas, S. Sadanandan, Y. K. Sharma, S. Chinthalapalli and A. Shandilya, *Tetrahedron Lett.*, 2012, **53**, 623–626.

21 V. Haridas, S. Sadanandan, M. V. S. Gopalakrishna, M. B. Bijesh, R. P. Verma, S. Chinthalapalli and A. Shandilya, *Chem. Commun.*, 2013, **49**, 10980.

22 K. Wüthrich, C. Spitzfaden, K. Memmert, H. Widmer and G. Wider, *FEBS Lett.*, 1991, **285**, 237–247.

23 N. H. Andersen, J. W. Neidigh, S. M. Harris, G. M. Lee, Z. Liu and H. Tong, *J. Am. Chem. Soc.*, 1997, **119**, 8547–8561.

24 S. Levinger, Y. Sharabi-Ronen, A. Mainfeld and A. Albeck, *J. Org. Chem.*, 2008, **73**, 7793–7796.

25 V. A. Palyulin, S. V. Emets, V. A. Chertkov, C. Kasper and H.-J. Schneider, *Eur. J. Org. Chem.*, 1999, **1999**, 3479–3482.

26 A. D. Bain, G. J. Duns, F. Rathgeb and J. Vanderkloet, *J. Phys. Chem.*, 1995, **99**, 17338–17343.

27 D. Kern, M. Schutkowski and T. Drakenberg, *J. Am. Chem. Soc.*, 1997, **119**, 8403–8408.

28 A. H. Andreotti, *Biochemistry*, 2003, **42**, 9515–9524.

29 J. S. Nowick, E. M. Smith and G. Noronha, *J. Org. Chem.*, 1995, **60**, 7386–7387.

30 J. S. Nowick, D. L. Holmes, G. Mackin, G. Noronha, A. J. Shaka and E. M. Smith, *J. Am. Chem. Soc.*, 1996, **118**, 2764–2765.

31 T. Cierpicki and J. Otlewski, *J. Biomol. NMR*, 2001, **21**, 249–261.

32 N. J. Baxter and M. P. Williamson, *J. Biomol. NMR*, 1997, **9**, 359–369.

33 Y. Zhang, Y. Zhong, A. L. Connor, D. P. Miller, R. Cao, J. Shen, B. Song, E. S. Baker, Q. Tang, S. V. S. R. K. Pulavarti, R. Liu, Q. Wang, Z. Lu, T. Szyperski, H. Zeng, X. Li, R. D. Smith, E. Zurek, J. Zhu and B. Gong, *J. Am. Chem. Soc.*, 2019, **141**, 14239–14248.

34 X. Daura, K. Gademann, B. Jaun, D. Seebach, W. F. van Gunsteren and A. E. Mark, *Angew. Chem., Int. Ed.*, 1999, **38**, 236–240.

35 A. Dong, P. Huang and W. S. Caughey, *Biochemistry*, 1990, **29**, 3303–3308.

36 A. M. Woys, A. M. Almeida, L. Wang, C.-C. Chiu, M. McGovern, J. J. de Pablo, J. L. Skinner, S. H. Gellman and M. T. Zanni, *J. Am. Chem. Soc.*, 2012, **134**, 19118–19128.

37 S. Pal, in *Fundamentals of Molecular Structural Biology*, Elsevier, 2020, pp. 119–147.

38 S. Chowdhury, G. Schatte and H.-B. Kraatz, *Angew. Chem., Int. Ed.*, 2008, **47**, 7056–7059.

39 D. E. Clarke, E. T. Pashuck, S. Bertazzo, J. V. M. Weaver and M. M. Stevens, *J. Am. Chem. Soc.*, 2017, **139**, 7250–7255.

40 L. Zhai, Y. Otani, Y. Hori, T. Tomita and T. Ohwada, *Chem. Commun.*, 2020, **56**, 1573–1576.

41 K. H. Mayo, E. Ilyina and H. Park, *Protein Sci.*, 1996, **5**, 1301–1315.

42 E. Marcos, T. M. Chidyausiku, A. C. McShan, T. Evangelidis, S. Nerli, L. Carter, L. G. Nivón, A. Davis, G. Oberdorfer, K. Tripsianes, N. G. Sgourakis and D. Baker, *Nat. Struct. Mol. Biol.*, 2018, **25**, 1028–1034.

43 N. Sawyer, A. M. Watkins and P. S. Arora, *Acc. Chem. Res.*, 2017, **50**, 1313–1322.

44 J. Hennetin, B. Jullian, A. C. Steven and A. V. Kajava, *J. Mol. Biol.*, 2006, **358**, 1094–1105.

45 Z. S. Derewenda, L. Lee and U. Derewenda, *J. Mol. Biol.*, 1995, **252**, 248–262.

46 R. W. Newberry and R. T. Raines, *Nat. Chem. Biol.*, 2016, **12**, 1084–1088.

47 F. Weinhold and C. R. Landis, *Valency and Bonding: A Natural Bond Orbital Donor-acceptor Perspective*, Cambridge University, Cambridge, 2005.

48 E. D. Glendening, A. E. Reed, J. E. Carpenter and F. Weinhold, *NBO Version 3.1*, Gaussian, Pittsburg, PA, CT, 2003.

49 D. Voet and J. G. Voet, *Biochemistry*, J. Wiley & Sons, New York, 2nd ed., 1995.

50 C.-I. Brändén and J. Tooze, *Introduction to protein structure*, Garland Publishing, New York, 2nd ed., 1999.

51 X. Li, L. Zhou, Y. Wei, A. M. El-Toni, F. Zhang and D. Zhao, *J. Am. Chem. Soc.*, 2015, **137**, 5903–5906.

52 Y.-M. Jeon, J. Kim, D. Whang and K. Kim, *J. Am. Chem. Soc.*, 1996, **118**, 9790–9791.

53 C. O. Mellet, J. M. G. Fernández and J. M. Benito, *Chem. Soc. Rev.*, 2011, **40**, 1586–1608.

54 D. T. Bong, T. D. Clark, J. R. Granja and M. R. Ghadiri, Self-Assembling Organic Nanotubes, *Angew. Chem., Int. Ed. Engl.*, 2001, **40**, 988–1011.

55 V. Haridas, *Acc. Chem. Res.*, 2021, **54**, 1934–1949.

56 A. Bhattacharya, R. J. Brea and N. K. Devaraj, *Chem. Sci.*, 2017, **8**, 7912–7922.

57 W. M. Aumiller, M. Uchida and T. Douglas, *Chem. Soc. Rev.*, 2018, **47**, 3433–3469.